Gemini: A Compact Yet Efficient Bi-Copter UAV for Indoor Applications

Youming Qin, Wei Xu, Adrian Lee, and Fu Zhang

***Abstract*—Quad-copters are the premier platform for data collection tasks, yet their ability to collect data in indoor narrow spaces is severely compromised due to their huge size when carrying heavy sensors. In this letter, we study a bi-copter UAV configuration that has similar levels of versatility and improves the compactness or efficiency at the same time. Such an arrangement allows for the preservation of propeller size, meaning that we can effectively reduce the horizontal width of the UAV while still maintains the same payload capacity. Furthermore, pitch, roll and yaw control can also be achieved through mechanically simple means as well, increasing reliability and precision. We also found that the Gemini platform is the most power-efficient yet practical solution for indoor applications among all the twelve common UAV configurations. This letter will detail the entire process of creating the platform from picking the ideal propeller through aerodynamic analysis, system design, optimization, implementation, control, and real flight tests that demonstrate its ability to function seamlessly.**

***Index Terms*—Aerial systems: mechanics and control, field robots, indoor UAV, bi-copter.**

I. Introduction

DUE to the inherent mechanical simplicity and superior mobility, quad-copters have emerged as the premier platform for a multitude of tasks such as inspection, indoor construction site mapping, exploration, post-disaster search & rescue [1]–[3]. These tasks are often performed by on-board sensors such as LiDAR and professional cameras, which tend to be as heavy as they are precise. While most quad-copters increase the size of their propellers to compensate for the extra mass, their ability to operate indoors or in tight spaces is in turn severely compromised. Indoor applications usually demand high payload capacity along with a small size, while having sufficient endurance to finish tasks [4]. Many tasks require a few hundred grams payload of 3D LiDAR, the size of a corridor or a human body width (with necessary safety clearance) and more than 10 minutes fly time. These three requirements conflict with each other and fundamentally limit the applicability of quad-copters.

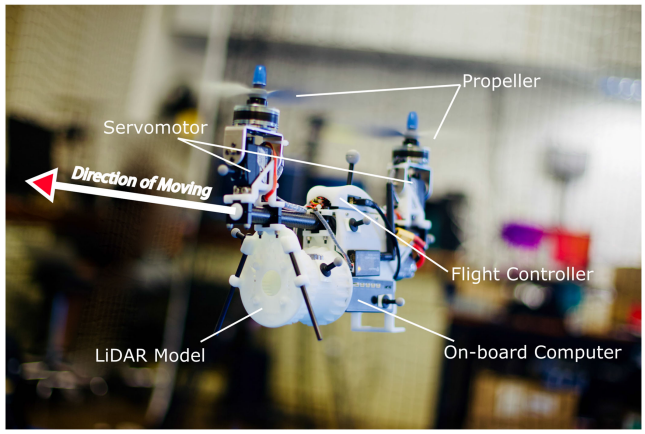

Fig. 1. The Gemini at Hovering. (The propeller size is 10 inches. By moving in the direction indicated by the arrow, the Gemini has a compact size of the propeller diameter, making it suitable for flying in congested indoor environments. It carries a 3D LiDAR sensor and a powerful on-board computer, which allows it to perform tasks like real-time 3D LiDAR mapping. The total system weighs 1.8 kg, and is capable of flying up to 13 minutes) Video is available at https://youtu.be/i7n0wOHonMM.

For example, the DJI Matrice M100 can carry up to 0.9 kg of extra payloads, yet it has a wingspan of 806 mm [5], which is considerably larger than the average width of a door in indoor operations. An intuitive approach may seem like to reduce the size of the UAV such that it can fit through a door frame, yet, the UAV has to be able to carry a sufficiently heavy payload, and decreasing its size will greatly diminish its ability to do so. Take another example, Crazyflie 2.0, a miniature quad-copter UAV, is capable of fitting through extremely small gaps [6]. However, its maximum payload mass is a meager 15 g.

Previous solutions to the problem of flying through confined spaces have been done. One simple solution is making use of the flat geometry of a quad-copter and rolling the whole UAV to fit a narrow gap [7], [8]. Besides requiring accurate trajectory calculation and tracking, this maneuver cannot be constantly maintained (e.g., flying through a long narrow corridor) as rolling will inevitably cause lateral movement. In addition, the nature of this approach also limits the amount of space below the UAV that payloads can be mounted on, as the height of a UAV would surely interfere with the maneuver. Adaptive morphology is another solution of enabling a UAV to adapt to confined spaces. D. Falanga *et al.* [9] transforms the frame of the UAV into different configurations to allow it to fit through a space that it may not have been able to previously. This solution allowed UAVs to maintain their

Manuscript received September 9, 2019; accepted January 28, 2020. Date of publication February 18, 2020; date of current version March 5, 2020. This letter was recommended for publication by Associate Editor J. Roberts and A. Elfes upon evaluation of the reviewers' comments. This work was supported in part by a DJI donation and in part by the HKU staff startup fund. *(Corresponding author: Youming Qin.)*

Youming Qin, Wei Xu, and Fu Zhang are with the Department of Mechanical Engineering, University of Hong Kong, Hong Kong 00852, China (e-mail: qym96@hku.hk; xuweii@connect.hku.hk; fuzhang@hku.hk).

Adrian Lee is with the Department of Mechanical and Aerospace Engineering, University of California, Davis, CA 95616 USA (e-mail: adree@ucdavis.edu).

Digital Object Identifier 10.1109/LRA.2020.2974718

size without sacrificing power and efficiency. However, the degree of deformation and the overall UAV size are still constrained by the many propellers being used. Moreover, the four additional servomotors also increase the mechanical complexity and UAV weight. To even decrease the UAV size, Riviere *et al.* [10] proposed a morphing mechanism that arranges all the four rotors in a row, reducing the UAV size to the size of a single propeller. However, with such a transformation, the roll axis is not controllable. Another application of such adaptive morphology can be found in [11]. Whereas the research above morphed the UAV across a single plane, that being lateral, the design of [11] contracts the arms of the UAV downwards into a ball, allowing it to halve its effective size. This configuration proves to be simpler than the previous one, as the morphing mechanism is passive, requiring no additional servomotors. However, similar to [9], the UAV in the morphed shape is inherently unstable and cannot be constantly maintained due to the loss of controllability. In summary, a majority of these suggested solutions tend to rely on unconventional concepts and mechanical prowess, which is generally not a reliable combination for practical uses in the current stage.

Our approach is a tandem rotor bi-copter UAV, as shown in Fig. 1. The bi-copter UAV uses two servomotors to produce torques in roll (tilt in the same direction) and yaw (tilt in opposite direction), and motor thrusts to produce pitch torque (differential thrust) and lift force (collective thrust). When compared to deformable quad-copter mentioned previously, this configuration is mechanical simpler (with the minimal set of actuators, i.e., two rotors, and two servomotors), smaller (reducing the UAV size to that of a single propeller), fully controllable (attaining full controllability in all flights), and more practical (carrying significant payloads for a prolonged time).

The concept of bi-copter with tilting rotors is not new, besides a variety of large manned aircraft of the bi-copter configuration [12]–[16], a vast amount of prior work can be found on small scale bi-copters, especially on their modeling and control. Sanchez *et al.* [17] first developed a prototype of such a bi-copter UAV concept, called T-Phoenix, and demonstrated its hover flight with a nonlinear controller. Papachristos *et al.* [18], Hrečko *et al.* [19], and Zhang *et al.* [20] focus on the attitude control of a model of Bell Boeing V-22 Osprey, which has two tilting rotors like Gemini but different moving direction. The position control in these works was not considered. Gonçalves *et al.* [21] presented a conceptual design of a similar bi-copter UAV, but with no actual prototype or test. While these works are all based on bi-copter UAVs with tilting rotors, Blouin *et al.* [22] proposed a UAV without any tilting mechanism. Due to the insufficient number of DOF in control, the UAV is not able to hover, which is essential for practical indoor applications. Siddhardha *et al.* [23] also presented a bi-copter UAV, which uses reaction wheels instead of servomotors to provide the roll and yaw torque. As claimed by the author, it is suitable for UAV with a very small moment of inertia on the roll axis. However, the work did not supply any actual test nor prototype of this design. Moreover, for actual bi-copter UAVs with payload, the moment of inertia on the roll axis is much significant and the torque provided by the reaction wheel is far sufficient for satisfactory control performance.

In this letter, we address the issue of flying through tight spaces through an adapted, optimized bi-copter UAV design. Unlike the existing work which focuses more on the control of such bi-copter UAV, we focus on the overall aircraft design and implementation to increase its usability, i.e., payload capacity, size, and power efficiency. More specifically, our contributions are threefold: (1) we conduct comprehensive aerodynamic analysis and show that the bi-copter UAV is the most power-efficient drone among all the common practical configurations for indoor applications; (2) we implement the concept of the UAV from systematically selecting its components (e.g., propeller, motors) to designing a simple yet effective control system that is composed of cascaded PID controllers with accurate control mixing. The prototype, known as the Gemini, has a compact size of 10 inches. It can operate for more than 13 minutes while carrying a full load of 500 g. We believe such results will have a practical impact on various field applications such as indoor 3D mapping, disaster response, exploration, etc.; (3) We demonstrate the whole system through real flight tests and validate its power consumption, payload capacity, maneuverability, and flight stability.

The remainder of this letter is organized as follows: Section II illustrates the aerodynamic analysis, comparison against various configurations, and the process of optimizing the efficiency. Section III covers the critical on-board elements that allow the Gemini to work seamlessly. The control system design will be detailed in Section IV. Last but not least, the experiment results, conclusion and future work will be presented in Section V and VI.

II. Aerodynamic Analysis

A. Momentum Theory

The momentum theory provides a mathematical model of an ideal actuator disk [24]. Let A be the rotor disk area, which can be measured by the area swept by the blades of a rotor, and ρ be the density of the air, then the power P required for the disk to produce thrust T in the ideal case is [24]

$$P = T \cdot \sqrt{\frac{T}{2A\rho}} \tag{1}$$

In characterizing the efficiency of an aircraft lifted by propellers (e.g., helicopter), the hover efficiency, HE, and disk loading, DL, are commonly used. They are defined as

$$DL = \frac{m}{A} \tag{2}$$

$$HE = \frac{m}{P} \tag{3}$$

where m is the aircraft mass. At hovering state, the propeller thrust is equal to the gravity, then, substituting (2) and (3) into (1) yields

$$HE = \frac{1}{g \cdot \sqrt{\frac{g}{2\rho} \cdot DL}} \tag{4}$$

Equation (4) implies that the hover efficiency is inversely proportional to the square root of disk loading: a lower disk loading leads to a higher efficiency.

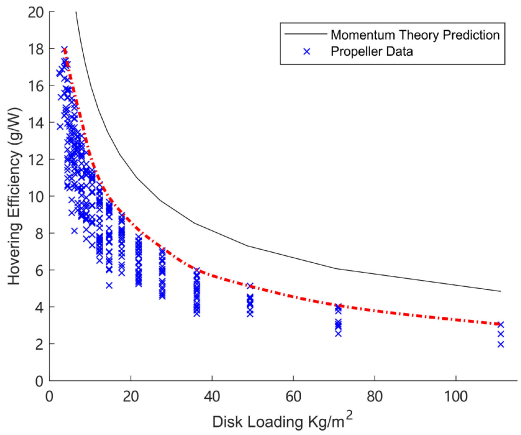

Fig. 2. Hover efficiency versus disk loading predicted by the momentum theory and from actual propeller data.

B. Experiment Verification

The relation predicted by the momentum theory in (4) did not consider any of the ground effects as shown in [25]. Many of the key propeller parameters such as airfoil, blade pitch, twist, and rotation speed, etc. are not modeled either. To verify this relation, we compare it to actual test data provided by the propeller manufacturers. In this letter, we restrict our attention to APC propellers due to the availability of its propeller data [26]. Fig. 2 summarizes how the hover efficiency changes with the disk loading from the theoretical predictions by (4) (the black curve) and actual propeller data (marked as "x"). When plotting the data points for actual propeller data, we fix the propeller thrust to 0.9 kg and compute the hover efficiency for all APC propellers. For propellers of the same size, they have different power consumption (thus different hover efficiency) due to the variation in airfoils, twist, pitch angles, etc., but the same disk loading, forming a perfect column of data points as shown in Fig. 2.

From Fig. 2, we notice that the envelope comprised of the highest data point in each column form a curve that is almost parallel to the theoretical predictions by (4), meaning that the momentum theory can successfully predict the actual performance of a properly designed propeller, and provide a simple yet effective model for our subsequent efficiency analysis. A constant gap between the envelope and the theoretical predictions is observed due to the unmodeled propeller parameters (e.g., airfoil, blade pitch and twist). Nevertheless, this constant gap does not change the relative efficiency among different propellers.

C. Efficiency Comparison

Based on the momentum theory explained and verified in the previous sections, we conduct a thorough comparison of our bi-copter against other possible UAV configurations. As an example, we analyze the power consumption of the Gemini bi-copter against a quad-copter with the same takeoff weight and effective size. In this case, the thrust produced by each propeller for a bi-copter at hovering T_2, and that of a quad-copter T_4 are related as

$$T_2 = 2 \cdot T_4 \tag{5}$$

Since the bi-copter moves along its longitudinal direction, the effective size of the whole UAV size is counted as one propeller diameter (as shown in Fig. 3). Then with the same effective size, the propeller radius of a bi-copter, r_2, and a quad-copter, r_4, are related as

$$r_2 = 2 \cdot r_4 \tag{6}$$

Substituting (5) and (6) into (1), and noticing that the total power is the power of a single propeller times the number of propellers, we have

$$\frac{P_2}{P_4} = \frac{\sqrt{2}}{2} \approx 0.71 < 1 \tag{7}$$

where P_2 and P_4 are the total power consumption of the bi-copter and the quad-copter configuration, respectively. The equation (7) implies that, with the same takeoff weight and UAV size, a bi-copter UAV consumes 30% less power than a quad-copter, theoretically. Or equivalently, with the same power consumption and takeoff weight, the bi-copter is 30% smaller than that of a quad-copter.

More generally, we extend this analysis to other common multi-rotor configurations, including helicopter (one-propeller), tri-copter, hexa-copter, and octo-copter, each with a single propeller and two co-axial propellers along each axis. The power consumption of all the multi-rotor configurations under the same size and take-off weight are summarized in Fig. 4, where all the power is normalized by the single propeller helicopter configuration.

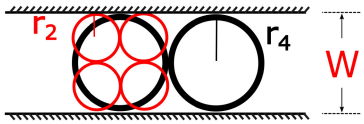

Fig. 3. The propeller radius of a bi-copter and a quad-copter with the same effective size.

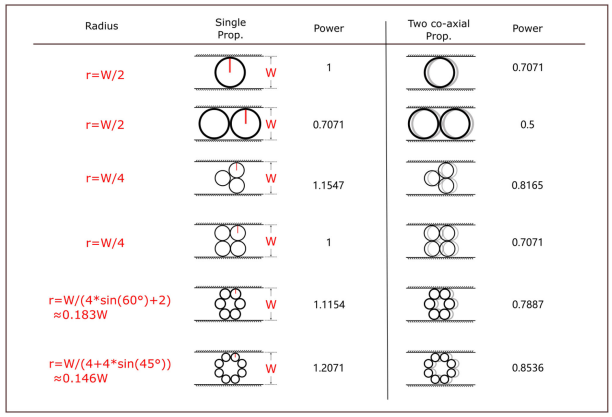

Fig. 4. Efficiency comparison among common multi-rotor UAVs. (The Gemini has the highest efficiency among the single propeller configurations, and it is also the most practical and mechanically simplest one among all configurations).

For UAVs that have only one propeller on an axis, it is clear that bi-copter consumes the least power. When considering the two co-axial propellers option, the co-axial bi-copter achieves even less power consumption than our bi-copter. Unfortunately, such configuration is not practically implementable: the two co-axial propellers (and associated motors) are too chunky to be installed on the same servomotor without any mechanical interference. The next optimal configurations among the co-axial option are the co-axial helicopter and co-axial quad-copters, which achieve the same efficiency as that of our bi-copter. However, since two co-axial propellers are usually less efficient than two individual propellers (like our bi-copter) because of one propeller being operating in the downstream of another [27], the power efficiency of these two configurations are usually considerably lower than the theoretical prediction in Fig. 4. Additionally, the co-axial helicopter has its propeller downstream being easily blocked by the payload and other mounting structures, and co-axial quad-copters suffer from various energy loss in motor and ESC due to the many propellers being used. Therefore, we conclude that the bi-copter is the most efficient configuration among these common UAV configurations under the same takeoff weight and size. Finally, the hexa-copter and octo-copter configurations listed in Fig. 4 are not considered in practice for indoor applications, not just because more motors bring down the efficiency [28], but also the many propellers (and motors) bring too much weight and the size of each propeller needs to be impractically small to fit in the whole UAV size. It is important to mention that, Fig. 4 only summarizes the commonly seen UAV configurations. There are various other unconventional configurations, such as the Triangular Quadrotor in [29], the "Stackrotor" platform in [30] and the aerial robot dragon in [31]. Even with the chosen bi-copter configuration, one can always keep increasing its efficiency by adding more rotors on the servo motor. Nevertheless, the bi-copter UAV is the minimal implementation, which simplifies the mechanical design and increases the maneuverability in tight spaces like turning in sharp corners.

III. System Design, Optimization, And Implementation

This section details the design, optimization, and implementation of the bi-copter UAV concept proposed in the previous section. Fig. 1 shows the developed bi-copter UAV, which consists of the main air-frame, battery, propeller/motor, servomotor, and on-board computer. In the current exemplary design, the payload is a 16-line LiDAR (Ouster-16, weighing 380 grams) for indoor mapping uses. At the size of only 10 inches (25.4 cm), the rated UAV takeoff weight is up to 1.8 kg and flies more than 13 minutes with a Dualsky 5000 mAH 4 s battery. The following Subsections detail the design of each component.

A. Propulsion System

According to the momentum theory, the bigger size of the propeller means higher efficiency, but also restricts the maneuverability of the UAV due to size increment. To enable the UAV to operate in congested indoor environments with narrow doors, windows, and other unstructured spaces, we restrict the UAV size (i.e., the propeller diameter) below 10 inches. Fig. 5 shows the power consumption for all APC propellers when providing 0.9 kg thrust. The data are drawn from the manufacturer [26]. It is seen that the APC10x45MR achieves the smallest power consumption. We also considered three-blades propellers in choosing the propeller. As shown in Fig. 5, three-blades propellers provide large thrusts with very small size (i.e., below 5 inches). However, when the propeller size increases, they are less efficient than two-blades propellers [27].

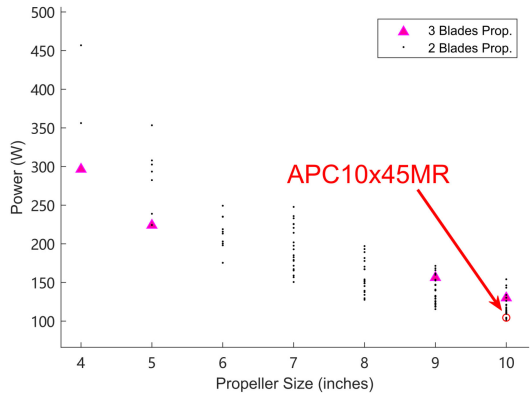

Fig. 5. Power consumption of all APC propellers below 10 inches. The propeller loading is 0.9 kg.

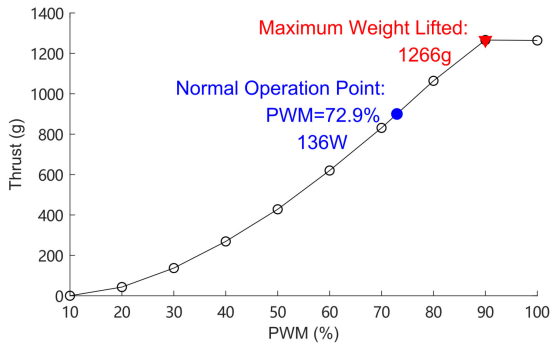

Fig. 6. Static thrust of the chosen propulsion system at different PWM input.

We use a T-Motor MT3506 650KV brush-less motor after a few trial tests. Fig. 6 shows the static thrust with the chosen motor and propeller. It is seen that by providing a maximal thrust up to 1.25 kg per propeller, the hover duty is 73%, leaving sufficient margin for maneuvering. The power consumption at hovering is $2 \times 136 = 272$ W. To show the effectiveness of the bi-copter, we make a trivial comparison to a quad-copter with well-designed propellers such as DJI snail 5048S propellers [32]. This propeller has a 5 inches diameter and leads to the same size if four are used. Reading data from [32], we obtain that a single DJI snail 5048S propeller consumes 142 W when providing 0.45 kg thrust. As a consequence, the quad-copter will consume 568 W, more than twice of a bi-copter.

We use a 4S 5000 mAh battery, Dualsky 30 C. Its high C rating allows a large current to be drained, as is the case of Gemini. Considering the 25 W of power consumption from other

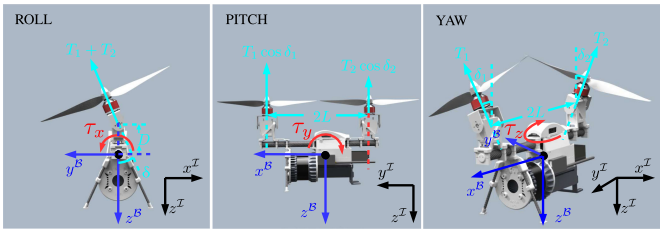

Fig. 7. The torque produced by the rotor thrusts: (a) Roll torque: $\tau_x = T_1 D \sin\delta_1 + T_2 D \sin\delta_2$ (b) Pitch torque $\tau_y = (T_1 \cos\delta_1 - T_2 \cos\delta_2) L$; (c) Yaw torque $\tau_z = (T_1 \sin\delta_1 - T_2 \sin\delta_2) L$.

electronics such as on-board computer, the estimated flight time is 15 minutes.

For the fast response of the Gemini, a servomotor with short response time is necessary. We chose the MKS HV1220, which has 0.115 seconds of response time and allows a higher control bandwidth. The titanium gearbox inside the motor also prevents malfunctioning from violent shocks. It is also able to overcome the Coriolis torque caused by propeller rotation by providing a torque up to 23 kg*cm.

B. Avionics

We use Pixhawk 4 mini as the flight controller hardware, but replaced the key controller software including mixer (see Section IV). A DJI Manifold 2 on-board computer is used to receive position feedback from motion capture systems and send this position feedback to the flight controller for position control. This on-board computer will also be used to process the LiDAR data and camera images to enable autonomous indoor operation in the future.

IV. Control

A. Dynamics

Fig. 7 shows the definition of the inertial frame ($\boldsymbol{x}^{\mathcal{I}}\boldsymbol{y}^{\mathcal{I}}\boldsymbol{z}^{\mathcal{I}}$) and body frame ($\boldsymbol{x}^{\mathcal{B}}\boldsymbol{y}^{\mathcal{B}}\boldsymbol{z}^{\mathcal{B}}$).[1] The inertial frame is in the convention of North-East-Down (NED). The UAV dynamics follow a standard rigid-motion:

$$\begin{bmatrix} m\boldsymbol{I} & 0 \\ 0 & \boldsymbol{J}^{\mathcal{B}} \end{bmatrix} \begin{bmatrix} \dot{\boldsymbol{v}}^{\mathcal{I}} \\ \dot{\boldsymbol{\omega}}^{\mathcal{B}} \end{bmatrix} + \begin{bmatrix} 0 \\ \widehat{\boldsymbol{\omega}}^{\mathcal{B}} \boldsymbol{J}^{\mathcal{B}} \boldsymbol{\omega}^{\mathcal{B}} \end{bmatrix} = \begin{bmatrix} \boldsymbol{f}_g \\ 0 \end{bmatrix} + \begin{bmatrix} \boldsymbol{R} \boldsymbol{f}_T^{\mathcal{B}} \\ \boldsymbol{\tau}^{\mathcal{B}} \end{bmatrix} \tag{8a}$$

$$\boldsymbol{R} = \boldsymbol{R}_z(\eta)\boldsymbol{R}_y(\theta)\boldsymbol{R}_x(\varphi) \tag{8b}$$

where m, $\boldsymbol{I}$ and $\boldsymbol{J}^{\mathcal{B}}$ stand for the mass, the identity matrix in $\mathbb{R}^{3\times3}$ and inertia matrix, $\boldsymbol{\omega}^{\mathcal{B}}$ is the angular velocity vector represented in the body frame while $\widehat{\boldsymbol{\omega}}^{\mathcal{B}}$ is the skew-symmetric cross product matrix of $\boldsymbol{\omega}^{\mathcal{B}}$, $\boldsymbol{v}^{\mathcal{I}}$ is the velocity vector represented in the inertial frame, $\boldsymbol{f}_g = [0\ 0\ mg]^T$ stands for the gravity in the inertial frame, $\boldsymbol{R}$ is the rotation matrix from the inertial frame to the body frame following the Z-Y-X Tait-Bryan order where η, θ, and φ stand for the yaw, pitch, and roll Euler angle, respectively,

[1]Throughout the text the superscript $^{\mathcal{I}}$ and $^{\mathcal{B}}$ will be used to denote the inertial and body frame, respectively.

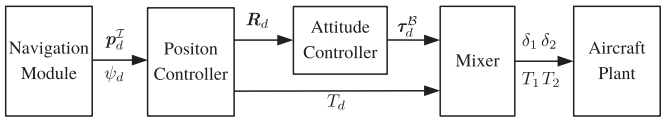

Fig. 8. The proposed controller structure.

$\boldsymbol{\tau}^{\mathcal{B}} = [\tau_x\ \tau_y\ \tau_z]^T$ is the moment vector produced by rotors in body frame, where τ_x, τ_y, τ_z are detailed in Fig. 7, the force vector is $\boldsymbol{f}_T^{\mathcal{B}} = [0\ 0\ T]^T$, where $T = T_1 \cos\delta_1 + T_2 \cos\delta_2$.

It should be noted that there are three simplifications in the above modeling process. (1) The reactive torque of servomotor, which comes from the angular acceleration of its rotor, is not modeled because the rotor inertia is quite small when compared to the whole aircraft. (2) The propeller torque is also ignored in $\boldsymbol{\tau}^{\mathcal{B}}$ as it is usually small when compared to the torque caused by thrusts. (3) In the calculation for the force vector $\boldsymbol{f}_T^{\mathcal{B}}$, the thrust projected to the y-axis of the body frame during the tilt of the two servomotors is neglected. This force is only present in the transient response of roll rotation and is zero when the roll angle converges to the desired value. The neglected torque and force will bring additional dynamics to the UAV rotation and translation and require careful modeling [17]. In this letter, we focus on designing the baseline controller that aims to stabilize the overall system. For this purpose, the three simplifications are valid, as shown in the actual experiments.

B. Control System

The whole control structure of Gemini is shown in Fig. 8. The navigation module produces the target position $\boldsymbol{p}_d$ and yaw angle ψ_d for position controller to track. The position controller will generate the desired attitude $\boldsymbol{R}_d$ and body-Z axis force T_d. The attitude controller will calculate the desired moment $\boldsymbol{\tau}_d^{\mathcal{B}}$ based on the desired attitude. And finally, the mixer will calculate the motor thrust commands and servo angle commands based on the $\boldsymbol{\tau}_d^{\mathcal{B}}$ and T_d.

1) Postition Controller: The position controller of Gemini is a cascaded controller with proportional gain K^p. It calculates the desired velocity $\boldsymbol{v}_d^{\mathcal{I}}$ as follows:

$$\boldsymbol{v}_d^{\mathcal{I}} = K^p \cdot \boldsymbol{p}_e^{\mathcal{I}} = K_p \cdot \left(\boldsymbol{p}_d^{\mathcal{I}} - \boldsymbol{p}^{\mathcal{I}}\right) \tag{9}$$

where $\boldsymbol{p}_e^{\mathcal{I}}$, $\boldsymbol{p}_d^{\mathcal{I}}$ and $\boldsymbol{p}^{\mathcal{I}}$ are the position error, desired position and current position, respectively. The inner velocity loop will calculate the desired acceleration $\boldsymbol{a}_d^{\mathcal{I}}$ through a PID controller:

$$\boldsymbol{v}_e^{\mathcal{I}} = \boldsymbol{v}_d^{\mathcal{I}} - \boldsymbol{v}^{\mathcal{I}} \tag{10a}$$

$$\boldsymbol{a}_d^{\mathcal{I}} = K_p^v \cdot \boldsymbol{v}_e^{\mathcal{I}} + K_i^v \cdot \int \boldsymbol{v}_e^{\mathcal{I}} + K_d^v \cdot \dot{\boldsymbol{v}}_e^{\mathcal{I}} \tag{10b}$$

where $\boldsymbol{v}_e^{\mathcal{I}}$ and $\boldsymbol{v}^{\mathcal{I}}$ are the velocity error and current velocity, respectively, K_p^v, K_i^v and K_d^v are the gains of PID terms. The desired attitude $\boldsymbol{R}_d$ and force $\boldsymbol{f}_{Td}^{\mathcal{B}} = [0\ 0\ T_d]^T$ can be uniquely solved from the below equation following the method in [33]:

$$m\boldsymbol{a}_d^{\mathcal{I}} = \boldsymbol{f}_g + \boldsymbol{R}_d \boldsymbol{f}_{Td}^{\mathcal{B}} \tag{11}$$

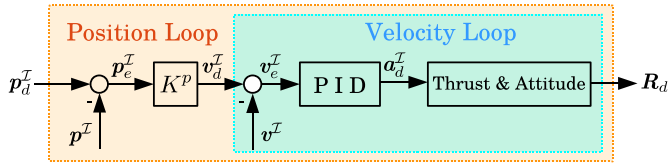

Fig. 9. The structure of position controller.

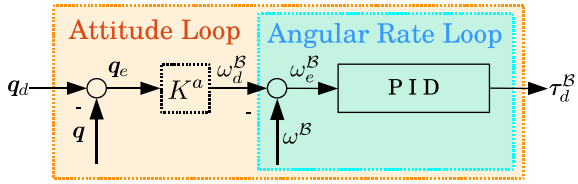

Fig. 10. The structure of attitude controller.

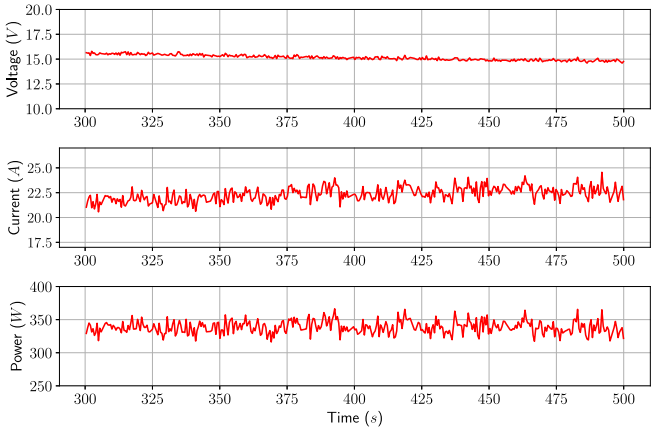

Fig. 11. The voltage, current, and power consumption during the hovering flight.

2) Attitude Controller: The attitude controller is also a cascaded controller. The outer loop (i.e., angular loop) is a proportional controller to track the desired attitude $\boldsymbol{R}_d$. The quaternion ($\boldsymbol{q} = [\eta, \boldsymbol{\epsilon}]$) is used to represent the attitude, where $\boldsymbol{\epsilon}$ and η denotes the vector and scalar part of the quaternion, respectively. With the quaternion representation, the attitude error $\boldsymbol{q}_e$ and desired angular velocity $\boldsymbol{\omega}_d^{\mathcal{B}}$ are calculated based on the "Quaternion linear" method in [34]:

$$\boldsymbol{q}_e = \boldsymbol{q}_d{}^* \otimes \boldsymbol{q} = \left[\eta_e \ \boldsymbol{\epsilon}_e^T\right]^T \tag{12a}$$

$$\varphi = 2 \cdot \operatorname{atan2}\left(\|\boldsymbol{\epsilon}_e\|, \eta_e\right) \tag{12b}$$

$$\boldsymbol{\omega}_d^{\mathcal{B}} = K^a \cdot \boldsymbol{\xi}_e^{\mathcal{B}} = K^a \cdot \operatorname{sign}\left(\eta_e\right) \frac{\varphi}{\sin(\frac{\varphi}{2})} \boldsymbol{\epsilon} \tag{12c}$$

where $\boldsymbol{q}_d$, $\boldsymbol{q}$ are the desired and actual attitude; K^a is the gain from attitude error $\boldsymbol{\xi}_e^{\mathcal{B}}$ to desired angular velocity $\boldsymbol{\omega}_d^{\mathcal{B}}$. The inner loop (i.e., angular rate loop) is a PID controller (13) to track the desired angular velocity $\boldsymbol{\omega}_d^{\mathcal{B}}$:

$$\boldsymbol{\omega}_e^{\mathcal{B}} = \boldsymbol{\omega}_d^{\mathcal{B}} - \boldsymbol{\omega}^{\mathcal{B}} \tag{13a}$$

$$\boldsymbol{\tau}_d^{\mathcal{B}} = K_p^r \cdot \boldsymbol{\omega}_e^{\mathcal{B}} + K_i^r \cdot \int \boldsymbol{\omega}_e^{\mathcal{B}} + K_d^r \cdot \dot{\boldsymbol{\omega}}_e^{\mathcal{B}} \tag{13b}$$

where $\boldsymbol{\omega}_e^{\mathcal{B}}$ and $\boldsymbol{\omega}^{\mathcal{B}}$ are the angular velocity error and current angular velocity, respectively. K_p^r, K_i^r and K_d^r are the gains of PID terms. The output of the inner loop is the desired moment $\boldsymbol{\tau}_d^{\mathcal{B}} = [\tau_{xd} \ \tau_{yd} \ \tau_{zd}]^T$.

3) Mixer: As shown in Fig. 7, the relationship between moments (τ_x, τ_y, τ_z), body-Z force T and actuator output (δ_1, δ_2, T_1, T_2) is as below:

$$\begin{bmatrix} 0 & 1 & 0 & 1 \\ D & 0 & D & 0 \\ 0 & L & 0 & -L \\ L & 0 & -L & 0 \end{bmatrix} \begin{bmatrix} T_1 \sin\delta_1 \\ T_1 \cos\delta_1 \\ T_2 \sin\delta_2 \\ T_2 \cos\delta_2 \end{bmatrix} = \begin{bmatrix} T \\ \tau_x \\ \tau_y \\ \tau_z \end{bmatrix} \tag{14}$$

Given desired moments $\boldsymbol{\tau}_d^{\mathcal{B}} = [\tau_{xd} \ \tau_{yd} \ \tau_{zd}]^T$ and desired body-Z force T_d, the actuator outputs δ_1, δ_2 and motor thrust outputs T_1, T_2 can be solved from (14) as:

$$\delta_1 = \operatorname{atan}\left(\frac{L \cdot \tau_{xd} + D \cdot \tau_{zd}}{D \cdot L \cdot T_d + D \cdot \tau_{yd}}\right) \tag{15a}$$

$$\delta_2 = \operatorname{atan}\left(\frac{L \cdot \tau_{xd} - D \cdot \tau_{zd}}{D \cdot L \cdot T_d - D \cdot \tau_{yd}}\right) \tag{15b}$$

$$T_1 = \frac{1}{2}\sqrt{\left(\frac{\tau_{xd}}{D} + \frac{\tau_{zd}}{L}\right)^2 + \left(T_d + \frac{\tau_{yd}}{L}\right)^2} \tag{15c}$$

$$T_2 = \frac{1}{2}\sqrt{\left(\frac{\tau_{xd}}{D} - \frac{\tau_{zd}}{L}\right)^2 + \left(T_d - \frac{\tau_{yd}}{L}\right)^2} \tag{15d}$$

V. Experiment Results

To validate the performance of the Gemini, a hovering flight with a disturbance test and a flying through 400 mm gap test are conducted. This section presents the experimental results obtained with our design and proposed controller.

A. Hovering Flight

Fig. 11 shows that the actual power consumption is around 335 W, which is 12.8% higher than our prediction of 297 W. The error is due to the downwash purling induced by the UAV body. With this power consumption, the estimated hovering time is 13.3 minutes with the 5000 mAh battery. The actual hovering time also depends on the battery discharging capabilities, the optimization of which is beyond the scope of this letter.

Fig. 12 shows that the position control is highly precise. Even with poking disturbances, the Gemini recovers within half a second, proving the robustness of the control system.

B. Flying Through a 400 mm Gap

To validate the preciseness and the stability of the Gemini, we challenged it to fly through a gap with a full payload. As shown in Fig. 13, two tall tripods are put together with 400 mm distance, and a motion capture system is used to give position feedback to the Gemini. The test process is to let the UAV hover in front of the two poles and accelerate at the x direction. The

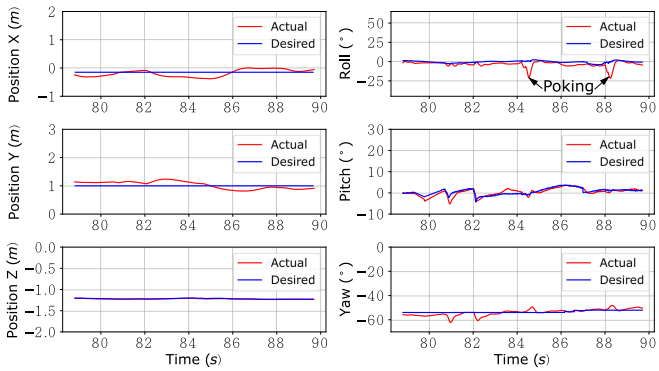

Fig. 12. The position and attitude during the hovering flight.

Fig. 13. Top, side and back view of the Gemini flying through a gap.

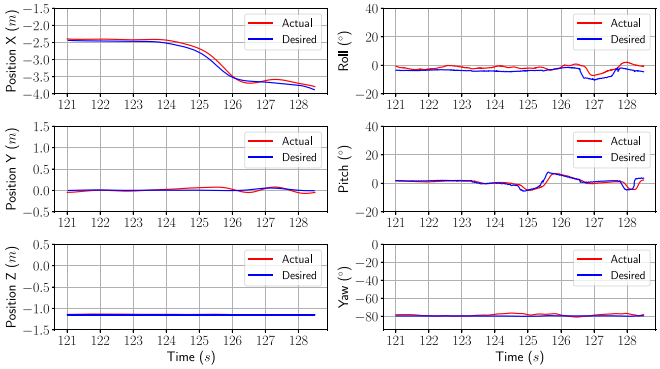

Fig. 14. The position and attitude when crossing the gap.

success of this experiment marks its ability to perform tasks in narrow spaces with no previous adaptations.

Fig. 14 shows the flight data when crossing the gap. The Gemini accelerated toward the x direction for 1 meter, while the other direction stays almost constant. The success of this challenge demonstrates the maneuverability of the Gemini.

VI. Conclusion and Future Work

This letter presents the design, analysis, implementation, and control of a bi-copter UAV. As demonstrated by flight experiments, the bi-copter platform proves to be stable in hover flight and is capable of carrying a significant payload. Our approach achieves similar levels of efficiency and maneuverability common amongst quad-copters and multi-rotor while allowing it to perform stable flight through small gaps. It should be noted that there are still multiple aspects of our design which can be improved upon. Immediately noticeable is the jerky yaw and roll control which is undoubtedly a result of a tandem-rotor bi-copter design. Also, the two additional dynamics as pointed out in the main texts need to be carefully modeled and compensated to achieve accurate and robust control of such a bi-copter UAV.

References

[1] Y. Khosiawan and I. Nielsen, "A system of UAV application in indoor environment," *Proc. Manuf. Res.*, vol. 4, no. 1, pp. 2–22, 2016.

[2] F. Nex and F. Remondino, "UAV for 3D mapping applications: A review," *Appl. Geomatics*, vol. 6, no. 1, pp. 1–15, 2014.

[3] V. Baiocchi, D. Dominici, and M. Mormile, "UAV application in post-seismic environment," in *Proc. Int. Arch. Photogr., Remote Sens. Spatial Inf. Sci.*, vol. 1, 2013, pp. 21–25.

[4] J. Senthilnath, M. Kandukuri, A. Dokania, and K. Ramesh, "Application of UAV imaging platform for vegetation analysis based on spectral-spatial methods," *Comput. Electron. Agriculture*, vol. 140, pp. 8–24, 2017.

[5] "DJI Matrice 100 user manual," 2016. [Online]. Available: https://dl.djicdn.com/downloads/m100/M100_User_Manual_EN.pdf

[6] W. Giernacki, M. Skwierczyński, W. Witwicki, P. Wroński, and P. Kozierski, "Crazyflie 2.0 quadrotor as a platform for research and education in robotics and control engineering," in *Proc. IEEE 22nd Int. Conf. Methods Models Autom. Robot.*, 2017, pp. 37–42.

[7] J. Lin, L. Wang, F. Gao, S. Shen, and F. Zhang, "Flying through a narrow gap using neural network: An end-to-end planning and control approach," 2019, *arXiv:1903.09088*.

[8] D. Falanga, E. Mueggler, M. Faessler, and D. Scaramuzza, "Aggressive quadrotor flight through narrow gaps with onboard sensing and computing using active vision," in *Proc. IEEE Int. Conf. Robot. Autom.*, 2017, pp. 5774–5781.

[9] D. Falanga, K. Kleber, S. Mintchev, D. Floreano, and D. Scaramuzza, "The foldable drone: A morphing quadrotor that can squeeze and fly," *IEEE Robot. Autom. Lett.*, vol. 4, no. 2, pp. 209–216, Apr. 2019.

[10] V. Riviere, A. Manecy, and S. Viollet, "Agile robotic fliers: A morphing-based approach," *Soft Robot.*, vol. 5, no. 5, pp. 541–553, 2018.

[11] N. Bucki and M. W. Mueller, "Design and control of a passively morphing quadcopter," in *Proc. IEEE Int. Conf. Robot. Autom.*, 2019, pp. 9116–9122.

[12] R. Bulaga and T. Worley, "UAV with control and stability system," U.S. Patent App. 11/746,628, Nov. 15, 2007.

[13] M. W. Moshier and R. W. Bulaga, "SoloTrek XFV(Exo-skeletor Flying Vehicle)- an inside look," in *Proc. Vertical Lift Aircr. Des. Conf., San Francisco, CA*, 2000.

[14] H. R. Stone and G. Clarke, "The T-wing: A VTOL UAV for defense and civilian applications," *University of Sydney*, 2001.

[15] B. Nordwall, "Boeing unveils heliwing UAV," *Aviation Week Space Technol.*, vol. 140, no. 14, pp. 34–34, 1994.

[16] B. Settle and T. Wise, "Bell Eagle Eye TR-911X–Tiltrotor unmanned aerial vehicle: Recent developments, autoland integration, and flight test demonstrations," *Annu. Forum Proc.-Amer. Helicopter Soc.*, vol. 56, no. 1, pp. 306–319, 2000.

[17] A. Sanchez, J. Escareno, O. Garcia, and R. Lozano, "Autonomous hovering of a noncyclic tiltrotor UAV: Modeling, control and implementation," *IFAC Proc. Volumes*, vol. 41, no. 2, pp. 803–808, 2008.

[18] C. Papachristos, K. Alexis, G. Nikolakopoulos, and A. Tzes, "Model predictive attitude control of an unmanned tilt-rotor aircraft," in *Proc. IEEE Int. Symp. Ind. Electron.*, 2011, pp. 922–927.

[19] L. Hrečko, J. Slačka, and M. Halás, "Bicopter stabilization based on IMU sensors," in *Proc. IEEE 20th Int. Conf. Process Control*, 2015, pp. 192–197.

[20] Q. Zhang, Z. Liu, J. Zhao, and S. Zhang, "Modeling and attitude control of bi-copter," in *Proc. IEEE Int. Conf. Aircr. Utility Syst.*, 2016, pp. 172–176.

[21] F. Gonçalves, J. Bodanese, R. Donadel, G. Raffo, J. Normey-Rico, and L. Becker, "Small scale UAV with birotor configuration," in *Proc. Int. Conf. Unmanned Aircr. Syst.*, 2013, pp. 761–768.

[22] C. Blouin and E. Lanteigne, "Pitch control of an oblique active tilting bi-rotor," in *Proc. IEEE Int. Conf. Unmanned Aircr. Syst.*, 2014, pp. 791–799.

[23] K. Siddhardha, "A novel bi-rotor configuration and its control," *IFAC-PapersOnLine*, vol. 51, no. 1, pp. 456–461, 2018.

[24] J. Leishman, "Principles of helicopter aerodynamics," Cambridge, U.K: Cambridge University Press, p. 36, 2008.
[25] E. Davis, J. Spollard, and P. Pounds, "Passive height stability and trajectory repeatability of a quadrotor maneuvering in ground effect with regulated voltage bus," in *Proc. Australas. Conf. Robot. Autom.*, 2015.
[26] "APC propeller performance data," 2019. [Online]. Available: https://www.apcprop.com/technical-information/performance-data/
[27] B. Theys, G. Dimitriadis, P. Hendrick, and J. De Schutter, "Influence of propeller configuration on propulsion system efficiency of multi-rotor unmanned aerial vehicles," in *Proc. IEEE Int. Conf. Unmanned Aircr. Syst.*, 2016, pp. 195–201.
[28] S. Salazar, H. Romero, R. Lozano, and P. Castillo, "Modeling and real-time stabilization of an aircraft having eight rotors," in *Unmanned Aircraft Systems*. Berlin, Germany: Springer, 2008, pp. 455–470.
[29] S. Driessens and P. Pounds, "The triangular quadrotor: A more efficient quadrotor configuration," *IEEE Trans. Robot.*, vol. 31, no. 6, pp. 1517–1526, Dec. 2015.
[30] E. Davis, W. McKay-Lowndes, D. Gonano, S. Hansen, and P. Pounds, "Towards the stackrotor: Aerodynamics, construction, dynamics and control of a vertical stacked-rotor configuration for indoor heavy-lift helicopter robots," in *Proc. Australas. Conf. Robot. Autom.*, 2016, vol. 2016, pp. 81–88.
[31] M. Zhao, T. Anzai, F. Shi, X. Chen, K. Okada, and M. Inaba, "Design, modeling, and control of an aerial robot dragon: A dual-rotor-embedded multilink robot with the ability of multi-degree-of-freedom aerial transformation," *IEEE Robot. Autom. Lett.*, vol. 3, no. 2, pp. 1176–1183, Apr. 2018.
[32] "Snail racing drone propulsion system - DJI." 2020. [Online]. Available: https://www.dji.com/hk-en/snail
[33] D. Mellinger and V. Kumar, "Minimum snap trajectory generation and control for quadrotors," in *Proc. IEEE Int. Conf. Robot. Autom.*, 2011, pp. 2520–2525.
[34] X. Lyu, H. Gu, J. Zhou, Z. Li, S. Shen, and F. Zhang, "A hierarchical control approach for a quadrotor tail-sitter VTOL UAV and experimental verification," in *Proc. IEEE IEEE/RSJ Int. Conf. Intell. Robots Syst.*, 2017, pp. 5135–5141.